

Regulation of Zn/Sn ratio in kesterite absorbers to boost 10% efficiency of $Cu_2ZnSn(S, Se)_4$ solar cells

Xue Min(闵雪), Jiangjian Shi(石将建), Linbao Guo(郭林宝), Qing Yu(于晴), Pengpeng Zhang(张朋朋), Qingwen Tian(田庆文), Dongmei Li(李冬梅), Yanhong Luo(罗艳红), Huijue Wu(吴会觉), Qingbo Meng(孟庆波), Sixin Wu(武四新)
Citation: Chin. Phys. B . 2018, 27(1): 016402. **doi:** 10.1088/1674-1056/27/1/016402

Journal homepage: http://cpb.iphy.ac.cn; http://iopscience.iop.org/cpb

What follows is a list of articles you may be interested in

First-principles hybrid functional study of the electronic structure and charge carrier mobility in perovskite $CH_3NH_3SnI_3$

Li-Juan Wu(伍丽娟), Yu-Qing Zhao(赵宇清), Chang-Wen Chen(陈畅文), Ling-Zhi Wang(王琳芝), Biao Liu(刘标), Meng-Qiu Cai(蔡孟秋)
Chin. Phys. B . 2016, 25(10): 107202. **doi:** 10.1088/1674-1056/25/10/107202

Effect of CuPc and MoO_3 co-evaporated layer on the conductivity of organic light emitting diodes

He Ze-Shang, Yu Hao-Miao, Peng Huan, Hou Xiao-Yuan
Chin. Phys. B . 2015, 24(9): 097201. **doi:** 10.1088/1674-1056/24/9/097201

Electric field-induced hole injection-enhanced photoluminescence in a N,N'-bis(3-methylphenyl)-N,N'-bis(phenyl)-benzidine-based emitter

Xu-Xie Hui-Na, Li Wen-Bin, Peng Huan, He Yun, Yu Hao-Miao, Hou Xiao-Yuan
Chin. Phys. B . 2014, 23(4): 047202. **doi:** 10.1088/1674-1056/23/4/047202

Combined frequency- and time-domain photocarrier radiometry characterization of ion-implanted and thermally annealed silicon wafers

Ren Sheng-Dong, Li Bin-Cheng, Gao Li-Feng, Wang Qian
Chin. Phys. B . 2013, 22(5): 057202. **doi:** 10.1088/1674-1056/22/5/057202

Degradation and recovery properties of AlGaN/GaN high-electron mobility transistors under direct current reverse step voltage stress

Shi Lei, Feng Shi-Wei, Guo Chun-Sheng, Zhu Hui, Wan Ning
Chin. Phys. B . 2013, 22(2): 027201. **doi:** 10.1088/1674-1056/22/2/027201

SPECIAL TOPIC — New generation solar cells

Regulation of Zn/Sn ratio in kesterite absorbers to boost 10% efficiency of $Cu_2ZnSn(S, Se)_4$ solar cells*

Xue Min(闵雪)[1,2], Jiangjian Shi(石将建)[1,2], Linbao Guo(郭林宝)[1,2], Qing Yu(于晴)[1,2], Pengpeng Zhang(张朋朋)[1,2], Qingwen Tian(田庆文)[3], Dongmei Li(李冬梅)[1,2], Yanhong Luo(罗艳红)[1,2], Huijue Wu(吴会觉)[1,2], Qingbo Meng(孟庆波)[1,2,†], and Sixin Wu(武四新)[3,‡]

[1] *Key Laboratory for Renewable Energy (CAS), Beijing Key Laboratory for New Energy Materials and Devices, Institute of Physics, Chinese Academy of Sciences, Beijing* 100190, *China*

[2] *School of Physical Sciences, University of Chinese Academy of Sciences, Beijing* 100049, *China*

[3] *The Key Laboratory for Special Functional Materials of MOE, Henan University, Kaifeng* 475004, *China*

(Received 17 October 2017; revised manuscript received 13 November 2017; published online 13 December 2017)

The Zn/Sn ratio in $Cu_2ZnSn(S, Se)_4$ (CZTSSe) films has been regulated to control the composition-related phase, defect, and photoelectric properties for high performance kesterite solar cells. It is found that the increase in the Zn/Sn ratio can slightly narrow the energy band gap to extend the light absorption range and improve the photocurrent. Optimal Zn/Sn ratio of 1.39 in CZTSSe film is obtained with the least secondary phase, the lowest defect density, and the longest charge recombination lifetime. Up to 10.1% photoelectric conversion efficiency has been achieved by this composition regulation.

Keywords: CZTSSe solar cell, composition regulation, defect suppression

PACS: 64.75.St, 72.20.Jv, 78.20.–e **DOI:** 10.1088/1674-1056/27/1/016402

1. Introduction

Kestertite materials such as Cu_2ZnSnS_4 (CZTS), $Cu_2ZnSnSe_4$ (CZTSe), and $Cu_2ZnSn(S, Se)_4$ (CZTSSe) have drawn wide attention as a kind of promising light absorbers for thin film solar cells due to their earth-abundant component elements, appropriate and adjustable band gaps (from 1.0 eV to 1.5 eV), and high light absorption coefficients (greater than 10^4 cm^{-1}).[1–5] In the past two decades, numerous studies on these materials have been made and a variety of vacuum and non-vacuum routes have been developed for the material preparation.[6–8] Among different non-vacuum techniques, the solution processed film deposition method stands out due to its distinctive advantages of simplicity, high material utilization, and facile control of the material components, which makes it attractive as a promising approach for the low-cost and sustainable production of kesterite solar cells. Up to now, the highest efficiency of 12.6% for the kesterite cell has been achieved by a hydrazine based method.[9] However, hydrazine is a high-toxic and explosive chemical, which restricts its wide application. Thus, the exploitation of safe and environmental friendly methods is desired, and some nanocrystal and molecular-ink approaches have been developed.[10–13]

The major challenge faced by these methods is how to precisely control the phase and defects in the kesterite absorber because of their complicated chemical compositions compared to the hydrazine system. First-principles calculations point out that the kesterite can keep stable only in a narrow thermodynamics phase region and that secondary phases are extremely easy to form in the fabrication processes.[14] It has also been demonstrated that the phase and defect properties of this semiconductor are closely correlated with the chemical potentials of the elements, that is, material composition.[1,15] Thus, for further developing highly efficient solution based kestertite solar cells, efforts are of high necessity to understand and regulate the composition-related phase, defect, and photoelectric performance in these systems. However, complicated and unknown interactions inside these solution systems together with the volatilization of stannum and zinc components increase the complexity of the composition control.[16–22]

In this work, the thioglycolic acid/ethanolamine-based system is employed to fabricate the CZTSSe solar cells.[12] The Zn/Sn ratio is adjusted to explore the impact of the Zn content on the optical and electrical properties of CZTSSe films and the photovoltaic performance. It is found that the Zn/Sn ratio has little influence on the film morphology but narrows the optical band gap (E_g), as demonstrated by the light transmission and photoluminescence (PL) spectroscopies. In addition, the Raman spectra show that the phases are sensitive to the Zn content. Optimal Zn/Sn = 1.39 for the CZTSSe film with the least secondary phase is obtained. In the meantime, the CZTSSe film displays the lowest defect density, the largest depletion width of about 400 nm, and the longest car-

*Project supported by the National Natural Science Foundation of China (Grant Nos. 51627803, 51402348, 51421002, 51372270, and 51372272) and the Knowledge Innovation Program of the Chinese Academy of Sciences.

†Corresponding author. E-mail: qbmeng@iphy.ac.cn

‡Corresponding author. E-mail: wusixin@henu.edu.cn

© 2018 Chinese Physical Society and IOP Publishing Ltd

rier recombination lifetime. As high as 10.1% photoelectric conversion efficiency has been achieved by this composition regulation.

2. Experimental section

2.1. Materials

Thioglycolic acid ($HSCH_2COOH$, 98%), ethanolamine ($HOCH_2CH_2NH_2$, 99.0%), and 2-methoxyethanol ($HOCH_2CH_2OCH_3$, 99.5%) were purchased from Aladdin. Se particles (99.999%) were purchased from ZhongNuo Advanced Material (Beijing) Technology Co., Limited. CuO (99.99%, Zhongnuo), ZnO (99.99%, Sigma-Aldrich), and SnO (99.9%, Aladdin) were used as metal sources.

2.2. Preparation of precursor solutions

The precursor solution was prepared by following the previous work.[12] Briefly, the CuO, ZnO, and SnO were dissolved into a mixed solvent composed of 4 mL 2-methoxyethanol, 2 mL ethanolamine, and 1.2 mL thioglycolic acid, in which the total amount of CuO, ZnO, and SnO was kept at 3.96 mmol, the amount of CuO was 1.76 mmol, and those of ZnO and SnO were adjusted to control the ratio. A clear yellow solution was obtained after 120 min stirring on a 60 °C hot plate. Five precursor solutions with the Zn/Sn ratios of 1.0, 1.1, 1.2, 1.3, and 1.4, respectively, were prepared while the Cu/(Zn+Sn) ratio was maintained at 0.8. For clarity, the CZTSSe thin films derived from these solutions were labeled as R0, R1, R2, R3, and R4, respectively.

2.3. Fabrication of CZTSSe films and photovoltaic devices

CZTS precursor films were prepared by spin-coating the precursor solution onto molybdenum coated soda lime glass (SLG) substrates (Mo/SLG) at 3000 rpm and followed by an annealing process on a 330 °C hot plate for 2 min in a nitrogen-filled glovebox. The spin-coating step was repeated for five times to obtain a desired thickness. The CZTSSe absorber was formed in the selenization process, which was carried out in a rapid thermal processing (RTP) furnace. The CZTS precursor film and 1.0 g Se particles were put in a quasi-closed graphite box and then annealed at 540 °C for 15 min under nitrogen flow (10^5 Pa). CZTSSe absorber films for transmission and photoluminescence (PL) characterization were directly deposited on SLG substrates without a molybdenum layer by following the same process.

CZTSSe solar cells were fabricated with the structure of SLG/Mo/CZTSSe/CdS/ZnO/ITO/Ag. A CdS buffer layer with the thickness of 50 nm was deposited onto the CZTSSe absorber by the chemical bath deposition (CBD) method, then followed by the radio frequency (RF) sputtering of 50 nm ZnO and 250 nm ITO as the window layer. Finally, an Ag grid was deposited by thermal evaporation, yielding an active area of 0.18 cm^2 for each cell.

2.4. Characterization

The compositions of the CZTSSe precursor films and CZTSSe absorber films were determined by an energy dispersive x-ray fluorescence (XRF) spectrometer (EDX-7000, Shimadzu). X-ray diffraction (XRD) patterns of the as-prepared samples were collected on an x-ray diffractometer with Cu $K\alpha$ as the radiation source (Empyrean, PANaltical). The morphologies of the films and devices were obtained by a scanning electron microscopy (S4800-SEM, Hitachi) and an atomic force microscope (Multimode 8, Bruker). The transmission spectra were obtained by a UV-Vis-NIR spectrophotometer (UV-3600, Shimadzu). The steady-state PL spectra were obtained from a fluorescence spectrometer (FLS920, Edinburgh Instruments) with the time integration mode, where the film was excited by a 535 nm monochromatic light from a xenon lamp. The Raman spectra were collected by a Raman spectrometer (HR800, Jobin Yvon), using a 532 nm excitation laser.

Current density–voltage (J–V) characteristics of the cells were collected on Keithley 2400 SourceMeter under AM1.5 illumination (1000 $W{\cdot}m^{-2}$) from Zolix SS150A. The light intensity of the solar simulator was calibrated by a standard monocrystalline Si reference solar cell. The external quantum efficiency (EQE) was measured on an SCS100 test system, Zolix, where a xenon lamp and a bromine tungsten lamp were used as the light sources and a certified Si and InGaAs diode was used as the reference detector. The capacitance–voltage (C–V) and drive level capacitance profiling (DLCP) studies were conducted on an electrochemical workstation (Versa STAT3, Princeton). The C–V measurements were performed at different DC bias voltages ranging from −1.0 V to 0 V with a perturbation AC voltage of 50 mV at 100 kHz. The DLCP measurements were performed while changing the 100 kHz AC perturbation voltage from 20 mV to 140 mV and the DC bias voltage was set from 0 to −0.54 V. The transient photovoltage of the cells was measured by our lab-made setup, in which the cell was excited by 532 nm pulse laser (Brio, 20 Hz, 4 ns) with an ultralow light intensity of about 10 $nJ{\cdot}cm^{-2}$ and the photovoltage decay process was recorded by a digital oscilloscope (Tektronix, DPO 7104) with a input impedance of 1 MΩ.[23,24]

3. Results and discussion

3.1. CZTSSe absorber films

As we know, for an efficient cell, the Cu poor condition is desired.[9,14] Here, the Cu/(Zn+Sn) ratio in the precursor solution is kept at 0.8 while the Zn/Sn ratio is adjusted from 1.0 to 1.4. Firstly, the compositions of the selenized CZTSSe films and the corresponding precursor films on Mo/SLG substrates are determined by XRF, as shown in Table 1. As designed, the

Cu/(Zn+Sn) ratios (∼ 0.83) of the samples are similar to each other and the composition difference mainly lies in the Zn/Sn ratio. The Zn/Sn ratios of the R0–R4 precursor films are 1.13, 1.25, 1.37, 1.57, and 1.62, respectively, implying that some Sn is evaporated in the relatively low temperature annealing process.[25] In the selenization process, the Sn continues to lose, thus leading to the Zn/Sn ratio slightly increased. During this composition regulation, the S/(S+Se) ratios for different films are almost the same, indicating their similar selenization behavior.

Table 1. The composition (XRF), root mean square roughness (R_q), light transmission, and PL properties of the selenized CZTSSe films.

Absorber	Cu/(Zn+Sn)	Zn/Sn	S/(S+Se)	R_q/nm	E_g/eV	PL peak/eV	(E_g-PL peak)/eV
R0	0.84 (0.83*)	1.19 (1.13)	0.07 (–)	149	1.13	1.01	0.12
R1	0.84 (0.83)	1.28 (1.25)	0.07 (–)	182	1.12	1.00	0.12
R2	0.83 (0.83)	1.39 (1.37)	0.07 (–)	143	1.11	0.98	0.13
R3	0.83 (0.83)	1.58 (1.57)	0.07 (–)	165	1.10	0.96	0.14
R4	0.82 (0.82)	1.65 (1.62)	0.05 (–)	184	1.06	0.92	0.14

* The value in the parentheses is the composition of the precursor film.

The structural properties and phase compositions of the CZTSSe films are further characterized by using XRD patterns, whose diffraction intensities are normalized to the (112) peak. As shown in Fig. 1(a), for all the films, a set of diffraction peaks at 17.2°, 23.4°, 27.2°, and 45.3° are observed, which are corresponding to the (101), (110), (112), and (312) crystal planes of CZTSSe, respectively, in the meantime, no observable secondary phases such as $SnSe_2$ and Cu_2Se are found.[26,27] Besides, no peak shift can be observed for different Zn/Sn ratios, suggesting that the Zn/Sn ratio has no obvious influence on the lattice structure or parameters. The possible influence of the Zn/Sn ratio on the morphology of the CZTSSe films is further studied by SEM and AFM, and no obvious difference is observed. Here, the selenized CZTSSe (R2) film is taken as an example. According to the top-view SEM image in Fig. 1(b), the film shows grains with the sizes up to micrometers, and the grains are packed closely to each other without obvious voids. The cross-sectional SEM image shows a bilayer structure consisting of a bottom layer (∼ 1.1 μm) with densely packed fine grains and an upper layer (∼ 1.0 μm) with large grains, as shown in Fig. 1(c). Obviously, the Zn/Sn ratio has no obvious influence on the thickness ratio of the large grain layer and the fine grain layer. The surface grain structure and roughness are further determined by AFM. Figures 1(d) and 1(e) give the AFM morphology images of the R1 and R2 films as examples. The root mean square roughnesses (R_q) of these five films are listed in Table 1. In line with the SEM results, the AFM also gives similar surface morphologies and R_q is in the range of 140–185 nm. No obvious dependence of R_q on the Zn/Sn ratio is obtained. It is thus deduced that the Zn/Sn ratio has no influence on the crystal structure and film morphology of the CZTSSe films.

Despite these similarities and the same S/Se composition, the optical properties of the CZTSSe semiconductors have been changed unexpectedly by the Zn/Sn ratio. As the Tauc plots transformed from the transmittance spectra shown in Fig. 2(a), the absorption band edge is obviously red-shifted by increasing the Zn/Sn ratio. For the R0 (Zn/Sn: 1.19), the E_g is about 1.13 eV, which is narrowed by about 70 meV to 1.06 eV for the R4 (Zn/Sn: 1.65). This narrowing behavior is indeed beneficial to the photoelectric conversion in the NIR region and is further demonstrated by the steady-state PL

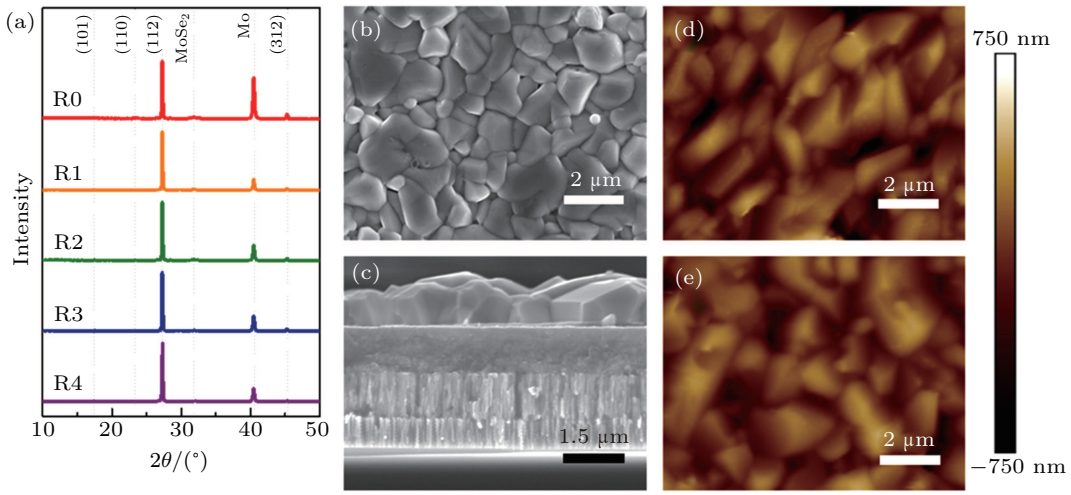


Fig. 1. (color online) (a) The XRD patterns of R0–R4 CZTSSe absorber films. (b) Top-view SEM image of R2 CZTSSe absorber film. (c) Cross-sectional SEM image of R2 CZTSSe absorber film. (d) AFM image of R1 CZTSSe absorber film. (e) AFM image of R2 CZTSSe absorber film.

measurement in Fig. 2(b). Here, the samples for PL measurements are directly deposited on SLGs, which present the similar XRF results. The PL peak energy decreases from 1.01 eV to 0.92 eV. For each film, the difference between the E_g and the PL peak is arisen from the band tail states and the Cu–Zn disorder effect is about 0.13 eV, indicating that the band-edge shallow defect properties of the CZTSSe are not influenced by the Zn/Sn ratio although the Cu/Zn ratio changes. For the CZTSSe system, the E_g is usually determined by the S/Se ratio and the lattice parameter,[28] but these values in our work do not change. Therefore, the mechanism behind the E_g adjustment still needs more clarification.

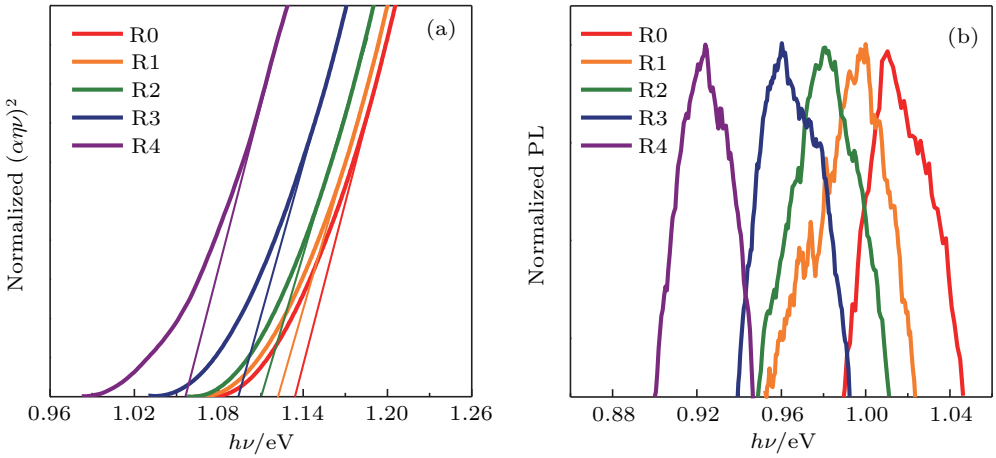


Fig. 2. (color online) (a) Tauc plots calculated from ultraviolet–visible transmission and measurements for R0–R4 CZTSSe absorber films. (b) Normalized PL spectra for R0–R4 CZTSSe absorber films.

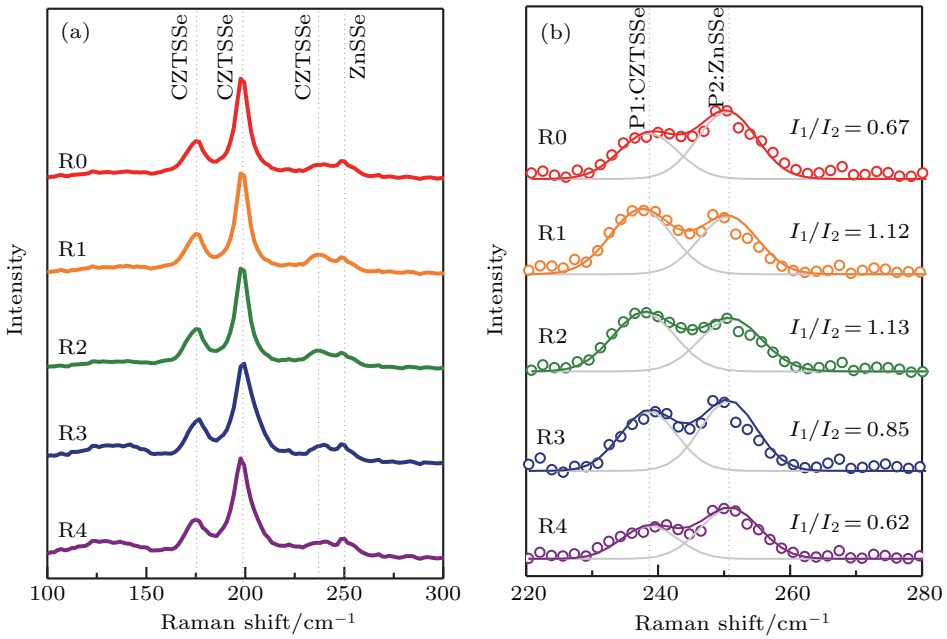


Fig. 3. (color online) (a) Normalized Raman spectra for R0–R4 CZTSSe absorber films. (b) Zoomed-in Raman spectra at the wave number from 220 cm^{-1} to 280 cm^{-1}.

The secondary phase is another issue concerned for the CZTSSe system, which is usually sensitive to the compositions.[14,29] Raman scattering spectroscopy is thus employed to distinguish the phases in the CZTSSe films. Raman spectra of these five samples are shown in Fig. 3(a) and the peak intensities are normalized to that of 197 cm^{-1} peak. The scattering peaks at 174 cm^{-1}, 197 cm^{-1}, and 237 cm^{-1} are attributed to the CZTSSe, in the meantime, the ZnSSe phase located at 251 cm^{-1} is also observed for all the samples.[30,31] Due to the complexity in our CZTSSe solution-processed method, this secondary phase is hardly avoided. ZnSSe is a wide bandgap semiconductor with ultralow electric conductivity, which is usually detrimental to the charge generation, transport and the device performance.[14,32] The relative content of the ZnSSe phase is obviously dependent on the Zn/Sn ratio. Figure 3(b) presents zoomed-in Raman spec-

tra ranging from 220 cm^{-1} to 280 cm^{-1}, which are fitted by the double-peak equations. The integrated intensities of the two peaks corresponding to CZTSSe (237 cm^{-1}) and ZnSSe (251 cm^{-1}) are labeled as I_1 and I_2, respectively. The I_1 of different samples has a constant proportion to that of the main peak at 197 cm^{-1}. And I_1/I_2 increases from 0.67 to 1.13 and then decreases to 0.62 with gradually increasing Zn/Sn ratio. R2 has the largest I_1/I_2, indicating its lowest ZnSSe content. The ZnSSe phase is suppressed by increasing the Zn amount in the first stage. It is probably due to the coexistence of multiple phases in the CZTSSe system with the help of the thermodynamics phase diagram. In the first stage of a Cu-poor/Sn-rich condition, the $Cu_2ZnSn_3(S,Se)_8$ could be formed after selenization although it is not observed from the XRD and Raman spectra, which is accompanied by the ZnSSe phase.[32] When increasing the Zn content, the Sn-rich condition gradually disappears, and purer CZTSSe is obtained with much less ZnSSe. However, when more Zn is involved, the ZnSSe phase appears again.[33] Thus, by regulating the Zn/Sn ratio, we can successfully control the secondary phase in the CZTSSe films, which could be beneficial for the device performance.

3.2. CZTSSe photovoltaic devices

With these CZTSSe films, the solar cell is fabricated by sequential depositions of CdS, ZnO, ITO, and Ag layers. Figures 4(a) and 4(b) give the *I*–*V* characteristics and EQE spectra of the best performance cells based on R0–R4 under the AM 1.5 illumination. Detailed parameters of the best performance device in each composition are listed in Table 2. The champion solar cell is based on the R2 composition, yielding a power conversion efficiency of 10.1% with V_{OC} of 409 mV, J_{SC} of 37.1 mA/cm^2, and FF of 0.664. To obtain a clearer relationship between the Zn/Sn ratio and the device performance, the performances of 18 cells are statistically shown as box-charts in Figs. 4(c)–4(f). It is clear that the averaged efficiency continuously increases from 7.5% to 9.8% when the Zn/Sn ratio changes from R0 to R2, then decays to about 1.8% when further increasing the Zn content to R4. Interestingly, the J_{SC}, V_{OC}, and FF exhibit similar dependence on the Zn/Sn ratio. For the J_{SC}, its improvement is derived from not only the light absorption extending to the longer wavelength region but also the enhancement in quantum efficiency in the short wavelength region, in good accordance with the EQEs. It seems that the evolution in the J_{SC} and FF is related to the amount of the ZnSSe secondary phase, but the series resistances derived from the *I*–*V* curves of different cells are similar to each other. This means that the enhancement in the device performance is not only dependent on the control of the insulating secondary phases. In terms of the change in the V_{OC}, the carrier recombination in the cell has been effectively suppressed.[34–36]

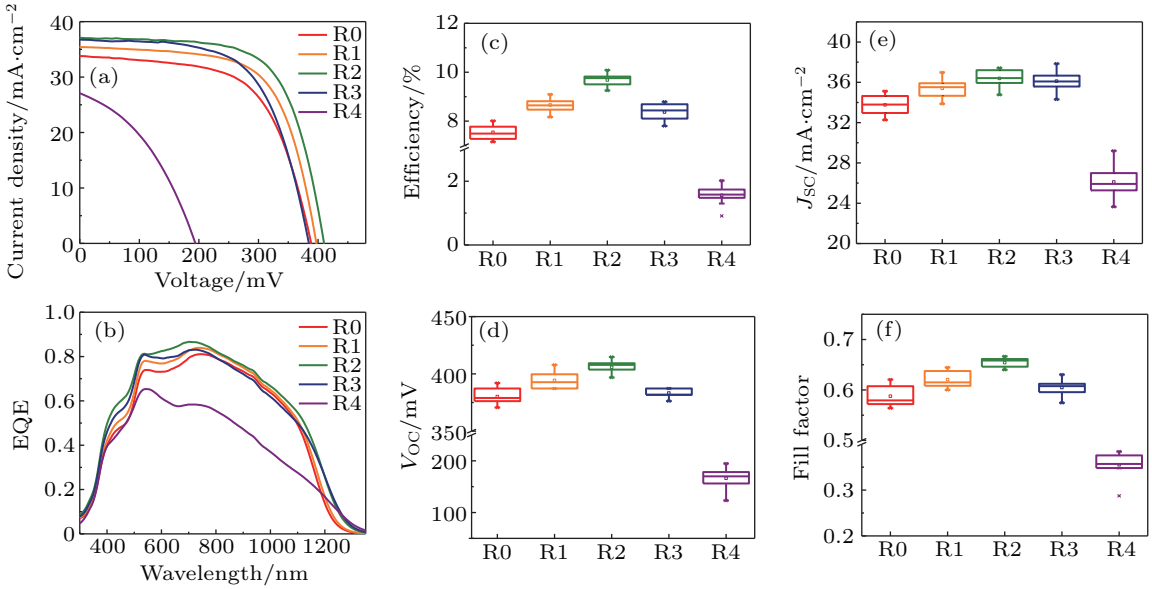


Fig. 4. (color online) (a) *J*–*V* curves and (b) EQE curves of best performance solar cells of R0–R4. (c) Efficiency, (d) open-circuit voltage, (e) short-circuit current density, (f) fill factor statistical box-charts for 18 solar cells of R0–R4.

Table 1. Photovoltaic performance characteristics of best performance solar cells of R0–R4.

Solar cell	PCE/%	V_{OC}/mV	J_{SC}/mA·cm^{-2}	Fill factor/%	R_{SH}/Ω·cm^2	R_S/Ω·cm^2
R0	8.01	387	33.7	61.2	116.8	2.0
R1	9.10	398	35.4	64.7	273.0	1.5
R2	10.08	409	37.1	66.4	178.3	1.5
R3	8.75	387	36.7	61.4	256.7	1.8
R4	2.02	195	26.9	38.4	22.9	3.2

The defect densities of CZTSSe absorbers and recombination properties of the cells are further evaluated by the capacitance (i.e., *C*–*V* and DLCP) and transient photovoltage measurements.[37,38] The electrical properties of R0–R4 solar cells are listed in Table 3. As seen in Fig. 5(a), the carrier and defect density of the CZTSSe absorber are significantly influenced by the Zn/Sn ratio. For the R0, its charge density at 0 V derived from the *C*-*V* (N_{CV}) is estimated to be 1.35×10^{16} cm^{-3}, in the same order to that obtained by the hydrazine method. Due to the avoidance of the defect charge response, the carrier density derived from the DLCP (N_{DLCP}) is a little lower, about 6.51×10^{15} cm^{-3}. The defect density at the interface (N_{IT}) is thus estimated to be about 7×10^{15} cm^{-3}, which can act as intermediate energy states for charge recombination or trapping, disadvantageous to the photoelectric conversion.[9] Fortunately, by regulating the Zn/Sn ratio, the N_{IT} is obviously suppressed under the R1 and R2 conditions, however, when further increasing the Zn content, the N_{IT} increases instead. For the R4 condition, the DLCP even cannot be reliably measured due to its poor performance. Based on the capacitance results, the width of the charge depletion region (W_d) is obtained, as depicted in Fig. 5(a). In line with the defect density, the W_d of the cell can be enhanced from 320 nm (R0) to 430 nm (R2). And this increase is supposed to be beneficial for the fast carrier transport across the CZTSSe absorber and thus helps to reduce the charge recombination probability.

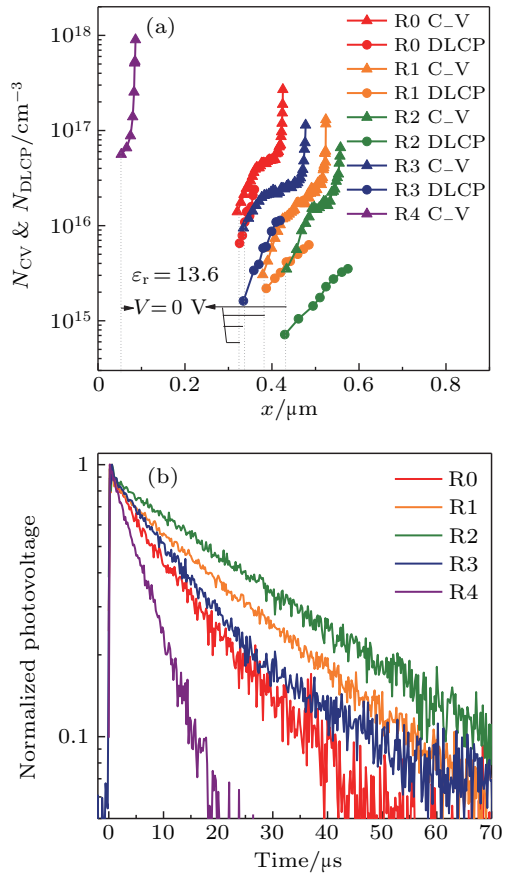


Fig. 5. (color online) (a) *C*–*V* and DLCP characteristics for R0–R4 solar cells. (b) Time-resolved transient photovoltage curves for R0–R4 solar cells.

To overcome the inaccuracy in the lifetime measurement by the PL, the transient photovoltage (TPV) method based on short-pulse laser and high-speed electrical detection is adopted to probe the charge recombination in the complete cell.[39] The photovoltage decay dynamics of the cells upon the nanosecond laser excitation are given in Fig. 5(b). All the cells exhibit a quasi-single exponential decay behavior, indicating a similar single-path recombination mechanism. The TPV lifetimes are obtained by fitting the spectra using a single exponential mode, and listed in Table 3. From R0 to R2, the lifetime is enhanced by about two times, from 14.2 μs to 29.0 μs, in good agreement with the N_{IT} results. It is thus suggested that the charge decay in this cell is mainly attributed to the defect-induced non-irradiative recombination. This suppression in the defect density and non-irradiative recombination can remarkably improve the cell performance when regulating the element composition.

Table 3. Electrical characteristics and TPV lifetimes of R0–R4 solar cells.

Absorber	W_d/μm	N_{CV}/cm^{-3}	N_{DLCP}/cm^{-3}	TPV τ/μs
R0	0.32	$1.35^{10}16$	$6.51^{10}15$	14.2
R1	0.39	$4.23^{10}15$	$2.18^{10}15$	22.8
R2	0.43	$3.68^{10}15$	$7.14^{10}14$	29.0
R3	0.33	$9.50^{10}15$	$1.61^{10}15$	14.5
R4	0.05	$5.79^{10}16$	–	7.5

4. Conclusion

In this work, the Zn/Sn ratio in the non-hydrazine system has been controlled for obtaining suitable optical and electrical properties of kesterite CZTSSe materials for highly efficient devices. It is found that increasing the Zn/Sn ratio can narrow the E_g of the CZTSSe semiconductor, which has contributed to the photoelectric conversion in the NIR region. Optimal Zn/Sn ratio of 1.39 is obtained with the least secondary phase, the lowest defect density, and the longest charge recombination lifetime. Based on these improvements, a high efficiency of 10.1% has been finally achieved.

References

[1] Chen S Y, Walsh A, Gong X G and Wei S H 2013 *Adv. Mater.* **25** 1522
[2] Polizzotti A, Repins I L, Noufi R, Wei S H and Mitzi D B 2013 *Energy Environ. Sci.* **6** 3171
[3] Zhou H P, Hsu W C, Duan H S, Bob B, Yang W B, Song T B, Hsu C J and Yang Y 2013 *Energy Environ. Sci.* **6** 2822
[4] Yan C, Sun K W, Huang J L, Johnston S, Liu F Y, Veettil B P, Sun K, Pu A, Zhou F Z, Stride J A, Green M A and Hao X J 2017 *ACS Energy Lett.* **2** 930
[5] Yang K J, Son D H, Sung S J, Sim J H, Kim Y I, Park S N, Jeon D H, Kim J S, Hwang D K, Jeon C W, Nam D, Cheong H, Kang J K and Kim D H 2016 *J. Mater. Chem. A* **4** 10151
[6] Haass S G, Diethelm M, Werner M, Bissig B, Romanyuk Y E and Tiwari A N 2015 *Adv. Energy Mater.* **5** 1500712
[7] Ahmed S, Reuter K B, Gunawan O, Guo L, Romankiw L T and Deligianni H 2012 *Adv. Energy Mater.* **2** 253
[8] Gershon T, Shin B, Bojarczuk N, Hopstaken M, Mitzi D B and Guha S 2015 *Adv. Energy Mater.* **5** 1400849

[9] Wang W, Winkler M T, Gunawan O, Gokmen T, Todorov T K, Zhu Y and Mitzi D B 2014 *Adv. Energy Mater.* **4** 1301465

[10] Guo Q J, Ford G M, Yang W C, Walker B C, Stach E A, Hillhouse H W and Agrawal R 2010 *J. Am. Chem. Soc.* **132** 17384

[11] Xin H, Vorpahl S M, Collord A D, Braly I L, Uhl A R, Krueger B W, Ginger D S and Hillhouse H W 2015 *Phys. Chem. Chem. Phys.* **17** 23859

[12] Tian Q W, Wang G, Zhao W G, Chen Y Y, Yang Y C, Huang L J and Pan D C 2014 *Chem. Mater.* **26** 3098

[13] Guo J, Zhou W H, Pei Y L, Tian Q W, Kou D X, Zhou Z J, Meng Y N and Wu S X 2016 *Sol. Energy Mater. Sol. Cells* **155** 209

[14] Kumar M, Dubey A, Adhikari N, Venkatesan S and Qiao Q 2015 *Energy Environ. Sci.* **8** 3134

[15] Shin D, Saparov B and Mitzi D B 2017 *Adv. Energy Mater.* **6** 1602366

[16] Katagiri H, Jimbo K, Tahara M, Araki H and Oishi K 2009 *MRS Proceedings* **1165** M04-01

[17] Tanaka K, Fukui Y, Moritake N and Uchiki H 2011 *Sol. Energy Mater. Sol. Cells* **95** 838

[18] Chawla V and Clemens B 2012 *Photovoltaic Specialists Conference (PVSC),* 38*th IEEE*, June 3–8, 2012, Austin, TX, USA, p. 002990

[19] Malerba C, Biccari F, Ricardo C L A, Valentini M, Chierchia R, Müller M, Santoni A, Esposito E, Mangiapane P and Scardi P 2014 *J. Alloys Compd.* **582** 528

[20] Li J J, Wang H X, Luo M, Tang J, Chen C, Liu W, Liu F F, Sun Y, Han J B and Zhang Y 2016 *Sol. Energy Mater. Sol.Cells* **149** 242

[21] Tao J H, Chen L L, Cao H Y, Zhang C J, Liu J F, Zhang Y B, Huang L, Jiang J C, Yang P X and Chu J H 2016 *J. Mater. Chem A* **4** 3798

[22] Larramona G, Levcenko S, Bourdais S, Jacob A, Choné C, Delatouche B, Moisan C, Just J, Unold T and Dennler G 2015 *Adv. Energy Mater.* **5** 1501404

[23] Shi J J, Xu X, Zhang H Y, Luo Y H, Li D M and Meng Q B 2015 *Appl. Phys. Lett.* **107** 163901

[24] Shi J J, Xu X, Li D M and Meng Q B 2015 *Small* **11** 2472

[25] Redinger A, Berg D M, Dale P J and Siebentritt S 2011 *J. Am. Chem. Soc.* **133** 3320

[26] Li J J, Zhang Y, Zhao W, Nam D, Cheong H, Wu L, Zhou Z Q and Sun Y 2015 *Adv. Energy Mater.* **5** 1402178

[27] Fan F J, Wu L and Yu S H 2014 *Energy Environ. Sci.* **7** 190

[28] He J, Sun L, Chen S Y, Chen Y, Yang P X and Chu J H 2012 *J. Alloys Compd.* **511** 129

[29] Just J, Sutter-Fella C M, Lützenkirchen-Hecht D, Frahm R, Schorr S and Unold T 2016 *Phys. Chem. Chem. Phys.* **18** 15988

[30] Li J J, Wang H X, Wu L, Chen C, Zhou Z Q, Liu F F, Sun Y, Han J B and Zhang Y 2016 *ACS Appl. Mater. Interfaces* **8** 10283

[31] Fella C M, Uhl A R, Romanyuk Y E and Tiwari A N 2012 *Phys. Status Solidi* **209** 1043

[32] Altamura G and Vidal J 2016 *Chem. Mater.* **28** 3540

[33] Fairbrother A, Fontané X, Izquierdo-Roca V, Placidi M, Sylla D, Espindola-Rodriguez M, López-Mariño S, Pulgarín F A, Vigil-Galán O, Pérez-Rodríguez A and Saucedo E 2014 *Prog. Photovoltaics* **22** 479

[34] Gershon T, Lee Y S, Antunez P, Mankad R, Singh S, Bishop D, Gunawan O, Hopstaken M and Haight R 2016 *Adv. Energy Mater.* **6** 1502468

[35] Fu J, Tian Q W, Zhou Z J, Kou D X, Meng Y N, Zhou W H and Wu S X 2016 *Chem. Mater.* **28** 5821

[36] Yu J L, Zheng Z M, Dong L M, Cheng S Y, Lai Y F, Zheng Q, Zhou H F, Jia H J, Zhang H 2017 *Chin. Phys. B* **26** 046802

[37] Barnes P 2002 *Charact. Mater.* 579

[38] Heath J T, Cohen J D and Shafarman W N 2004 *J. Appl. Phys.* **95** 1000

[39] Shi J J, Li D M, Luo Y H, Wu H J and Meng Q B 2016 *Rev. Sci. Instrum.* **87** 123107